International Journal of Mechanical, Industrial and Aerospace Sciences
ISSN: 2517-9950
Vol:6, No:8, 2012

Numerical Investigation of Instabilities in Free Shear Layer Produced by NS-DBD Actuator

Ilya Popov and Steven Hulshoff

Abstract—A numerical investigation of the effects of nanosecond barrier discharge on the stability of a two-dimensional free shear layer is performed. The computations are carried out using a compressible Navier-Stokes algorithm coupled with a thermodynamic model of the discharge. The results show that significant increases in the shear layer's momentum thickness and Reynolds stresses occur due to actuation. Dependence on both frequency and amplitude of actuation are considered, and a comparison is made of the computed growth rates with those predicted by linear stability theory. Amplitude and frequency ranges for the efficient promotion of shear-layer instabilities are identified.

Keywords—NS-DBD, plasma, actuator, flow control, instability, shear layer

I. Introduction

RECENT experiments with nanosecond dielectric barrier discharge (NS-DBD) actuators [1] have demonstrated their ability to influence airflow separation patterns at higher Reynolds numbers. The manner in which they do so, however, is not yet fully understood. A number of mechanisms for their effectiveness have been proposed, including the promotion of boundary layer transition, induction of a small but critical changes of momentum, and promotion of instabilities in the shear layer adjacent to the separated region. This paper focuses on the last of these proposed mechanisms, motivated by the experimental observation of large coherent structures appearing in the shear layer following NS-DBD actuation. Their coherency is related to the geometry of the actuator, which is constant along the span of wing tested. As a result, the initial behavior of the shear layer prior to break-up appears to be two-dimensional.

In order to study the effect of NS-DBD actuators in the absence of other factors present in the experiment, a generic two-dimensional laminar shear layer problem is proposed. As it is known that NS-DBD discharge produces a significant shock wave [2], [1], compressible Navier-Stokes simulations are employed for its investigation.

The presence of a shock wave suggests that there is fast gas heating in the area of the discharge, which has been confirmed by measurements of heat distribution in the discharge area [1]. This phenomenon can be explained by plasma kinetic model, proposed in [3]. In this study the actuator is modelled as a finite-duration source term in enthalpy equation.

The layout of the paper is the following: The actuator model is discussed in section II. Then the simulation set up is described in section III. The results are presented and discussed in section IV. Finally, conclusions are given in V.

Ilya Popov and Steven Hulshoff are with the Faculty of Aerospace Engineering, Delft University of Technology, Kluyverweg 1, 2629 HS Delft, The Netherlands

Work is supported by Plasma Technology Development BV., The Netherlands

II. Actuator model

The presence of a shock wave is a distinguishing property of NS-DBD actuator compared to other types of plasma actuators. On the other hand, the direct momentum input of the NS-DBD actuator to the flow was measured in [4] and was found to be small.

A coupled NS-DBD flow simulation was performed in [5], where authors were able to reproduce a shock wave pattern similar to that observed in the experiments. Simulation of the discharge based on fundamental plasma-kinetic principles itself is difficult task, however, and lends little to the fidelity of the over flow simulation owing to the large separation in time scales between the plasma and flow phenomena.

Therefore, modeling of the actuator in current work is focused on the thermal effects of the actuator. The actuator is modeled as a enthalpy source, with distribution constant in square discharge area of size 0.5 by 0.5 mm. The density of the enthalpy output is estimated given total energy input to the discharge, which has been directly determined in experiments by measuring voltage and current of the incident and reflected pulses in the feeding coaxial cable, and the approximate volume of the discharge. The base value used in the present work is energy density per pulse $A = 10^5\,\mathrm{J/m^3}$, corresponding to linear energy per unit span $E \sim 25\,\mathrm{mJ/m}$.

The dimensionality of the plasma discharge remains an open question. There are observations [6], [1], which show that the discharge itself is non-uniform along the actuator, but consists of the filaments of more dense discharge and areas of weaker discharge between them. This distribution depends on many parameters, such as voltage and duration of the pulse. The filaments produce individual shock waves, which at some distance from the discharge merge to produce a single envelope wave. In the present work, the discharge and its effects are assumed to be uniform in spanwise direction.

For the current simulations, the energy input is assumed to be uniform in time during energy deposition period τ. A value of $1\,\mu\mathrm{s}$ is used according to kinetic model estimations [3] and previous measurements. This actuation is repeated with period T, with corresponding repetition frequency F being in the range 100–1500 Hz, corresponding to the range used in experiments [7]. In all cases shown, the first discharge occurs 1 ms after the start of the simulation.

III. Simulation description

The simulation domain is a square two-dimensional box with outer dimensions of $0.2\,\mathrm{m} \times 0.2\,\mathrm{m}$. On the inflow boundary

the following velocity profile is applied:

$$U(y)|_{x=0} = \frac{1}{2}(U_1 + U_2) + \frac{1}{2}(U_2 - U_1)\tanh\frac{y}{d} \qquad (1)$$

where U_2 and U_1 are free-stream flow velocities above and below the shear layer, whereas d is a shear layer thickness parameter. In the current work, values used were: $U_2 = 30\,\mathrm{m/s}$, $U_1 = 5\,\mathrm{m/s}$, $d = 0.25\,\mathrm{mm}$, which roughly correspond to the experimental conditions.

Momentum thickness of the shear layer, defined as

$$\theta = \int_{-\infty}^{\infty} \frac{U - U_1}{U_2 - U_1}\left(1 - \frac{U - U_1}{U_2 - U_1}\right)\mathrm{d}y \qquad (2)$$

for the inlet profile is equal to $\theta = d/2 = 0.125\,\mathrm{mm}$. This gives value of Reynolds number

$$Re = \frac{(U_2 - U_1)\theta}{\nu} = 208 \qquad (3)$$

which corresponds to an unstable shear layer.

According to linear stability theory, the most unstable frequency is given by $f_\mathrm{n}\theta/\overline{U} = 0.032$ which for the inlet profile gives $f_\mathrm{n} = 4480\,\mathrm{Hz}$.

On the remaining boundaries, wave transmissive boundary conditions are used. Strong mesh coarsening is used in the vicinity of these boundaries, to ensure vortical structures are dissipated before leaving the domain.

The high resolution core of the mesh has a length of 30 mm in the flow-wise direction and a width of 10 mm. This size of the core is enough for the formation of vortices, and ends about the same position as the first vortex pairing occurs. Refining more of the downstream domain makes little sense, since in reality there would be strong 3D effects and transition to 3D turbulence, which would be missed by a 2D simulation. The influence of the downstream region on the dynamics in the core region was quantified using comparisons with simulations using a longer core region. These have shown that there are no significant effects if downstream coarsening begins after position $x = 25\,\mathrm{mm}$. Thus, in the current work, the region of interest is limited to $x \in [0, 25]\,\mathrm{mm}$, $y \in [-5, 5]\,\mathrm{mm}$.

For the simulations presented here, there were no sources of instability excitation other than the actuation and natural feedback from the evolving shear layer. The initial condition used for simulations was the same and was obtained as a result of separate long simulation without actuation.

IV. Results

A. Shock wave

The first phenomena which appears in simulation after the actuation is a double N shock wave. The first one is produced by discharge itself, whereas the second arises due to a reflection of the from the inflow boundary.

Using numerical microphones, wave arrival times at different positions have been used to estimate the wave propagation velocity along the midline of the shear layer. The results are presented in Table I.

In the Fig. 1, velocity is plotted vs. time for several stations, demonstrating propagation of the shock wave. The estimated values of the wave velocity lie between 360–400 m/s (the straight line on the figure represents constant velocity of 400 m/s).

TABLE I
Shock Wave Arrival Time and Velocities at Different Positions

No	x, mm	Arrival time, μs	Wave speed, m/s
1	1	0	—
2	2	2.5	399
3	5	10.5	374
4	10	24.1	369
5	15	37.3	376
6	20	50.4	384
7	25	63.9	369
8	30	76.9	383

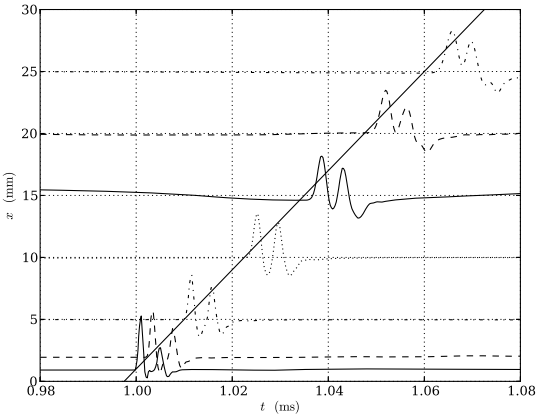

Fig. 1. Propagation of the shock wave along the shear layer. The line indicates a constant velocity $c = 400\,\mathrm{m/s}$. For every station normalized U is plotted over time.

B. Velocity oscillations and vortex structure

After the propagation of the shock wave, flow field becomes disturbed. This perturbations grow while convecting downstream in the form of vortical structures. An example of snapshot of the flow field is presented in the Fig. 2. Formed pair of vortices is similar to what have been observed in experiments [7].

Fig. 3, 4 and 5 represent time evolution of velocity at different positions (5 mm, 10 mm, and 20 mm respectively) for cases without actuation and with actuation at repetition frequencies of 667 Hz, 1000 Hz, and 1500 Hz.

It could be seen on the Fig. 3, which correspond to point $x = 5\,\mathrm{mm}$ that after each discharge (every shock wave is seen as a spike of velocity) flow velocity experiences a perturbation, which shape does not depend on the repetition frequency and is the same for every actuation repetition. Between actuation events the flow is undisturbed. This means that we have a coherent flow structures created by actuation event, which at this location do not interact with each other.

At next position, $x = 10\,\mathrm{mm}$ (Fig. 4), vortices produced at repetition frequency 1500 Hz start interact with each other, but yet without changing their shape. At lower frequencies, vortices remain separated from each other.

Further downstream, at $x = 20\,\mathrm{mm}$, vortices interact with each other at all presented repetition frequencies, and at this the difference in the shape is significant.

The described evolution corresponds well with the concept

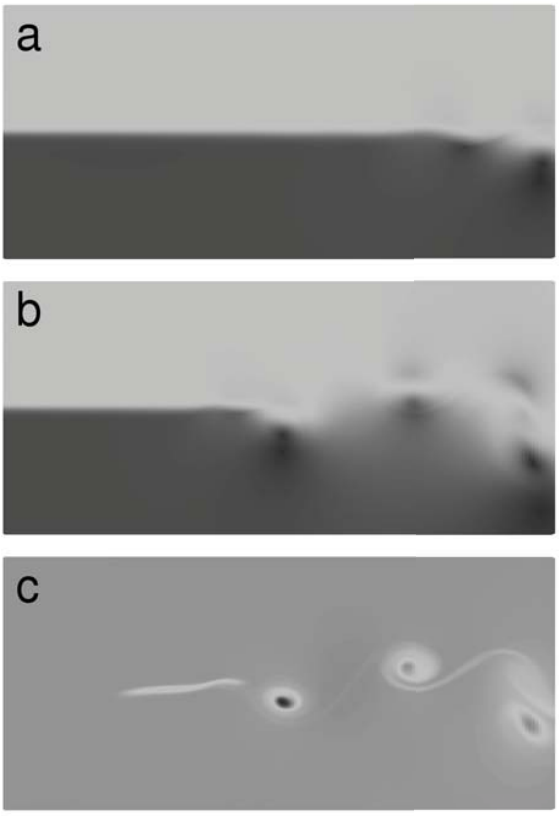

Fig. 2. Snaphots of flow field at time $t = 5\,\mathrm{ms}$. From top to bottom: a — magnitude of the velocity, reference case without actuation, b — magnitude of the velocity, actuation at 1000 Hz, c — density, actuation at 1000 Hz,

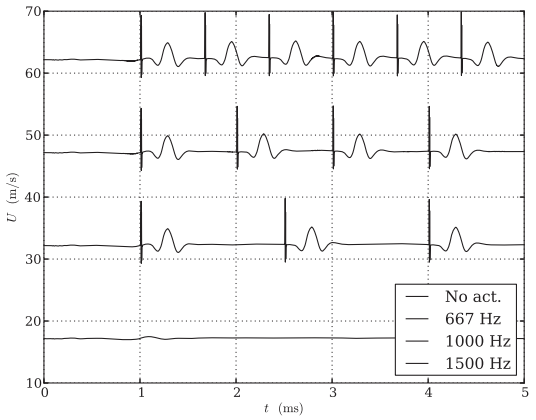

Fig. 3. Comparison of time evolution of U component of the velocity in the point 5 mm far from the inlet on the midline of the shear layer. Top to bottom: actuation at 1500 Hz, 1000 Hz, 667 Hz, no actuation

of convective instability. Fig. 6 illustrates this by showing

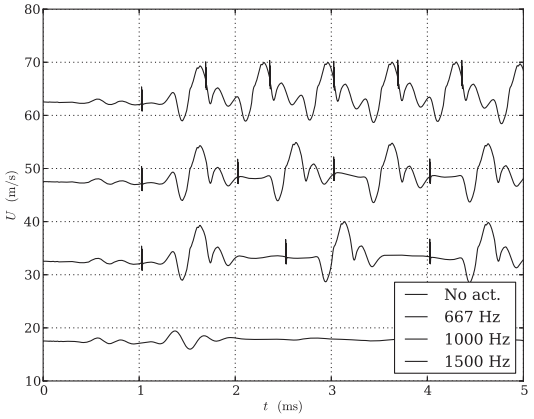

Fig. 4. Comparison of time evolution of U component of the velocity in the point 10 mm far from the inlet on the midline of the shear layer. Top to bottom: actuation at 1500 Hz, 1000 Hz, 667 Hz, no actuation

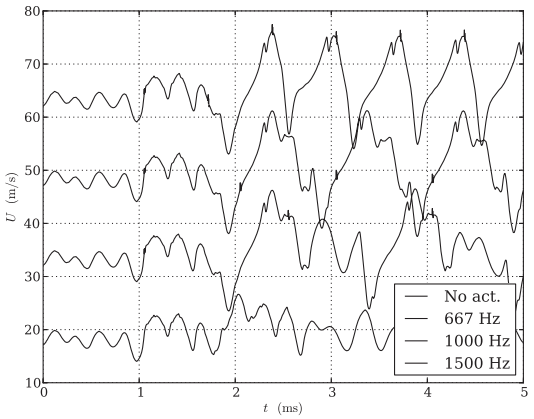

Fig. 5. Comparison of time evolution of U component of the velocity in the point 20 mm far from the inlet on the midline of the shear layer. Top to bottom: actuation at 1500 Hz, 1000 Hz, 667 Hz, no actuation

velocity versus time for several positions on the midline of the shear layer for one simulation. Here, propagation of the vortex could be seen, showing it's growth along streamwise direction and than merging of individual vortices into continuously disturbed flow. Straight lines indicate propagation of the head and the tail of the perturbation, with speeds 25 and 11 m/s, respectively. Thus the mean velocity of vortical disturbance propagation can be estimated as $\frac{1}{2}(25 + 11) = 18 \approx \bar{U}$. At this repetition frequency (1000 Hz) vortex interaction occurs at position $x \approx 15\,\mathrm{mm}$.

C. Entropy spot

After the discharge, there is a region of heated air which is convected with the flow. The motion of this region is correlated with the motion of the main vortex structure formed by the actuator. It can be seen in the Fig. 2 as a region with lower density. It is not clear for the moment if this "entropy spot"

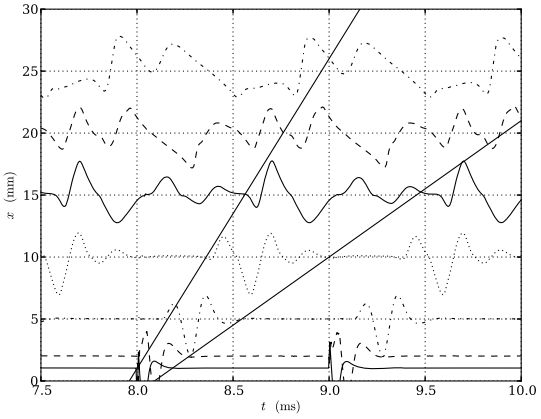

Fig. 6. Propagation of the vortex structure along the shear layer. Lines indicate constant velocities $c = 11\,\mathrm{m/s}$ and $25\,\mathrm{m/s}$. For every station normalized U is plotted over time.

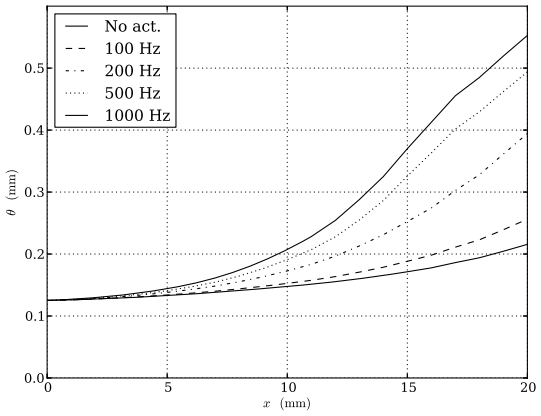

Fig. 7. Comparison of momentum thickness growth for cases without actuation and with actuation repetition frequency of 100 Hz, 200 Hz, 500 Hz and 1000 Hz.

plays any role in determining the main effects of the actuator.

D. Flow statistics

Dependence of momentum thickness of the shear layer on x coordinate is presented in Fig. 7, 8. It can be seen that momentum thickness grows much faster in the case of actuation. The growth is initially dependent on actuation frequency, but at higher frequencies saturation occurs. These seems to be caused by the strong interaction of vortical structures created in closely-spaced actuation events.

Components of the Reynolds stress tensor along the middle line of the shear layer are shown in the Fig. 9–14. The change in RMS variations caused by actuation is particularly significant.

It could be seen that at lower actuation frequencies ($F \leq 1000\,\mathrm{Hz}$) the growth of shear layer (as indicated both by momentum thickness and Reynolds stress) in monotonic, whereas at higher frequencies there is a point, after which thickness of shear layer growing slower, and Reynolds stresses increase no more. The higher the actuation frequency, the closer this effect is to the inlet. This affect can be attributed to coherent vortical structures caused by individual actuation events starting interacting with each other.

E. Comparison with linear stability theory

An unanswered question is if the same responses could be caused by excitations of a much simpler form. The computed disturbance growth rate in the frequency domain is therefore calculated and compared to linear stability theory. Fig. 15–18 show spectra of the computed velocity without actuation, and with actuation at different repetition frequencies.

In the absence of actuation the spectrum is continuous and there are no preferential frequencies. Once actuation is applied, almost all of the energy becomes contained in multiples of the actuation frequency. In the beginning, the envelope of the spectra have a maximum at about 4–5 kHz, independent of the actuation repetition rate. This corresponds to the most

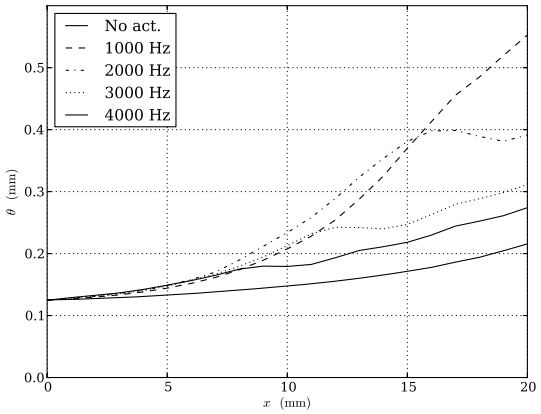

Fig. 8. Comparison of momentum thickness growth for cases with actuation repetition frequency of 1000 Hz, 2000 Hz, 3000 Hz and 4000 Hz.

unstable frequency of inlet shear layer profile. At stations further downstream, the maximum of the envelope of the spectrum shifts towards lower frequencies.

To compare the results more closely with linear stability theory, spatial growth rate coefficients have determined from the computed results. In linear stability theory, the disturbance to the mean flow is expressed in the form

$$\psi(x, y, t) = \phi(y)e^{i(ax-\omega t)} \tag{4}$$

where a is a spatial wavenumber and ω is an angular frequency. To identify these waves in the computed results a Fourier transform in time is used:

$$U(x, t) = \sum_j \hat{U}_j(x)e^{i\omega_j t} \tag{5}$$

where $\omega_j = 2\pi j f_0$, f_0 is the spectral resolution, and $\hat{U}_j(x)$ is Fourier component corresponding to frequency component number j. Given the Fourier transforms of the velocity at

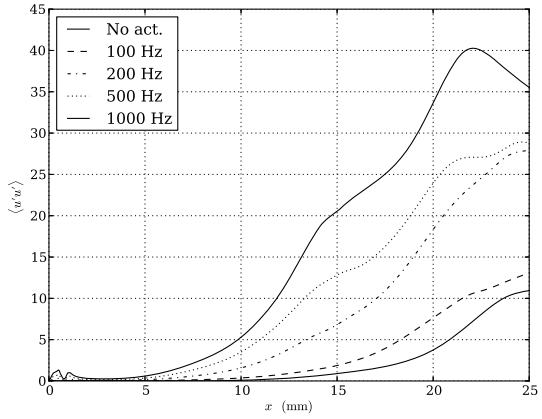

Fig. 9. Reynolds stress component $\langle u'u' \rangle$ along midline of the shear layer for cases without actuation and with actuation at 100 Hz, 200 Hz, 500 Hz and 1000 Hz repetition frequency.

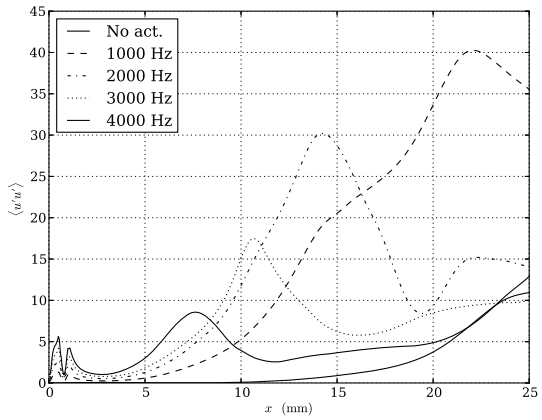

Fig. 10. Reynolds stress component $\langle u'u' \rangle$ along midline of the shear layer for cases without actuation and with actuation at 1000 Hz, 2000 Hz, 3000 Hz and 4000 Hz repetition frequency.

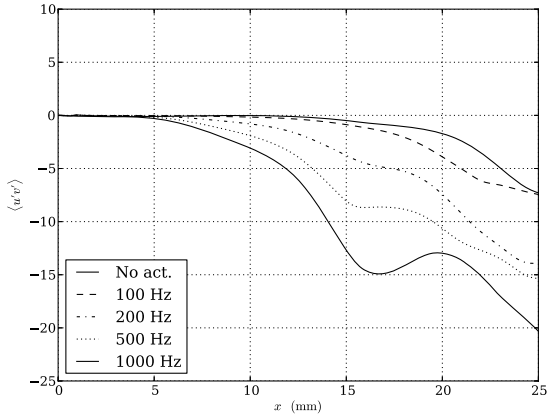

Fig. 11. Reynolds stress component $\langle u'v' \rangle$ along midline of the shear layer for cases without actuation and with actuation at 100 Hz, 200 Hz, 500 Hz and 1000 Hz repetition frequency.

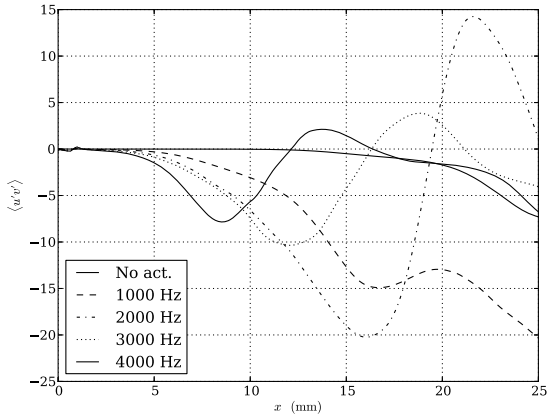

Fig. 12. Reynolds stress component $\langle u'v' \rangle$ along midline of the shear layer for cases without actuation and with actuation at 1000 Hz, 2000 Hz, 3000 Hz and 4000 Hz repetition frequency.

two points x and $x + \Delta x$, the complex wavenumber of jth frequency component can be estimated using

$$a_j = \frac{\partial}{\partial x} \log \hat{U}_j \approx \frac{\log \hat{U}_j(x + \Delta x) - \log \hat{U}_j(x)}{\Delta x} \tag{6}$$

and growth rate

$$g_j = -\operatorname{Im} a_j \tag{7}$$

Linear stability theory is normally expressed in terms of non-dimensionalized growth rate $g\theta/R$ (where $R = (U_2 - U_1)/(U_2 + U_1)$) and Strouhal number $St = f\theta/\bar{U}$. According to the theory, all the Strouhal numbers from 0 to 0.079 are unstable, the most unstable being $St = 0.032$ [8]. This depends only marginally on R. The growth rate of the most unstable frequency approximately equals $g_n\theta/R \approx 0.1$. Numerical procedure used to calculate theoretical growth rates is described in appendix.

Growth rates observed in simulation and predicted using linear stability theory (LST) are presented in Fig. Fig. 19. In the unstable range of frequencies ($0 < St < 0.08$) growth rate show come correspondence to predictions (especially at position $x = 5\,\mathrm{mm}$), but there are some systematic differences. In particular, the observed growth rate for low Strouhal numbers ($0 < St < 0.03$) tends to be higher than predicted, whereas in the range $0.04 < St < 0.08$ observed growth rates are lower than predicted. This indicates that the excitation due to actuation introduces new dynamics in the shear layer in addition to linear mechanism of instability growth.

Outside the instability region, at $St > 0.08$, the computed growth rates oscillate, reaching very high positive and large negative values. This can be attributed to the manner in which the growth rates are approximated. Firstly, the magnitudes of the Fourier transform themselves are very small in this region. Since the calculation of observed growth rates involves division

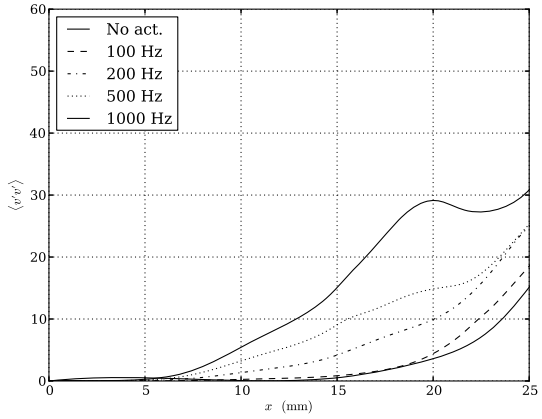

Fig. 13. Reynolds stress component $\langle v'v' \rangle$ along midline of the shear layer for cases without actuation and with actuation at 100 Hz, 200 Hz, 500 Hz and 1000 Hz repetition frequency.

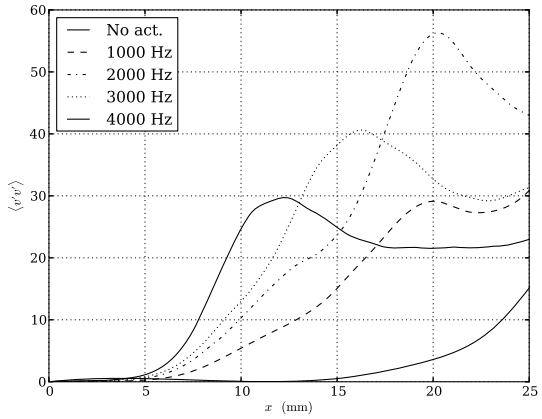

Fig. 14. Reynolds stress component $\langle v'v' \rangle$ along midline of the shear layer for cases without actuation and with actuation at 1000 Hz, 2000 Hz, 3000 Hz and 4000 Hz repetition frequency.

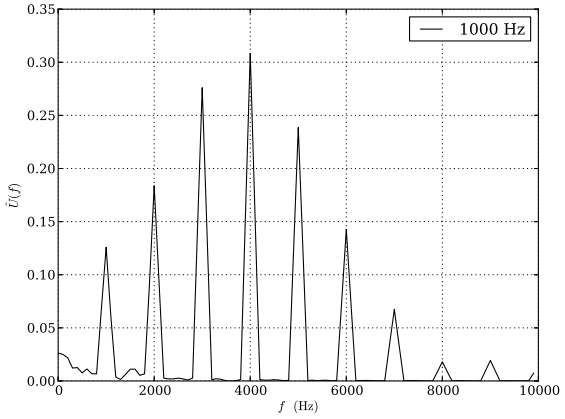

Fig. 15. Spectra of U component of the velocity in the point 5 mm far from the inlet on the midline of the shear layer.

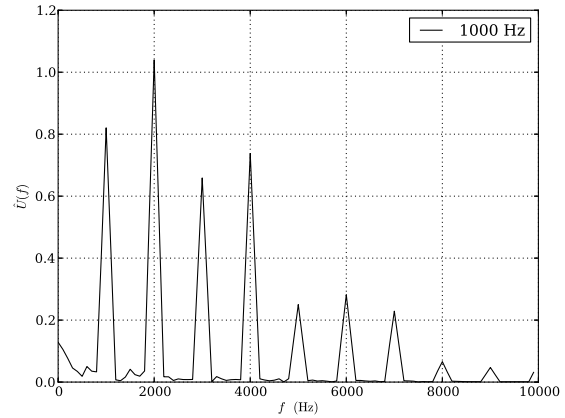

Fig. 16. Spectra of U component of the velocity in the point 10 mm far from the inlet on the midline of the shear layer.

of this magnitudes (equivalent to difference of logarithms), which leads to high errors of this growth rates. Secondly, there is the production of higher harmonics due to nonlinear effects, especially in the area of formation and pairing of small vortices, which occurs at $x > 15\,\mathrm{mm}$.

F. Effect of varying energy input

In addition to the frequency dependence, the dependence of the results on the energy input per pulse has been studied. Simulations with fixed repetition frequency of 1000 Hz and varying energy input per pulse have been carried out. Momentum thickness and Reynolds stress, as being considered most relevant characteristics of actuation effectiveness, are plotted over midline of the shear layer for several different values of energy per pulse and fixed repetition frequency $F = 1000\,\mathrm{Hz}$ in Fig. 20 and 21. The same characteristics for one fixed location $x = 10\,\mathrm{mm}$ are shown in Fig. 22 and 23 as functions of average discharge power $P = F \cdot E$, comparing with results obtained with fixed energy and varying repetition frequency. It can be seen that dependence of the results on energy per pulse is monotonic and smooth, whereas dependence on frequency exhibits a maximum, after which effectiveness decreases. Another interesting result is an almost exact equality of results at low average power levels, regardless if they reached by means of decreasing energy per pulse or repetition frequency.

Presented results can provide guidance for choosing optimal parameters of actuation in terms of energy efficiency. This is particularly important for practical applications, where discharge energy is limited by electric parameters of the equipment used, and thus can not be increased arbitrary. Consequently, there exists an optimal discharge frequency in terms effect onto parameters of shear layer such that momentum thickness and Reynolds stress at given maximum energy per pulse. It should be noted, however, that the value of that optimal frequency is not universal depends on the selected goal function (particularly, on which property we optimise for and

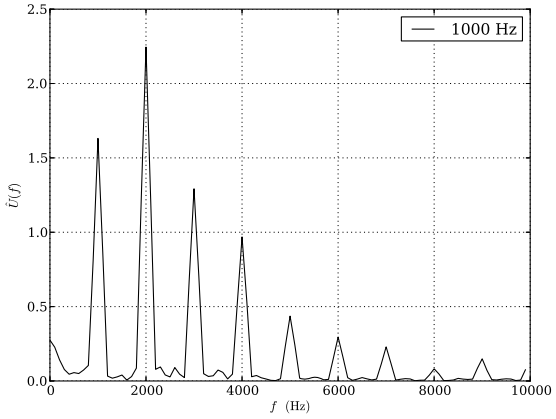

Fig. 17. Spectra of U component of the velocity in the point 15 mm far from the inlet on the midline of the shear layer.

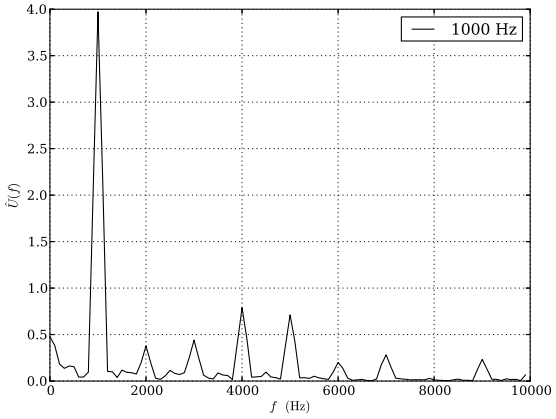

Fig. 18. Spectra of U component of the velocity in the point 20 mm far from the inlet on the midline of the shear layer.

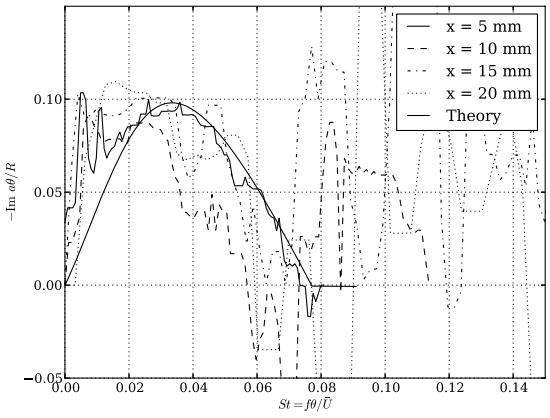

Fig. 19. Growth rate vs. Strouhal number for several x positions. Actuation at 667 Hz.

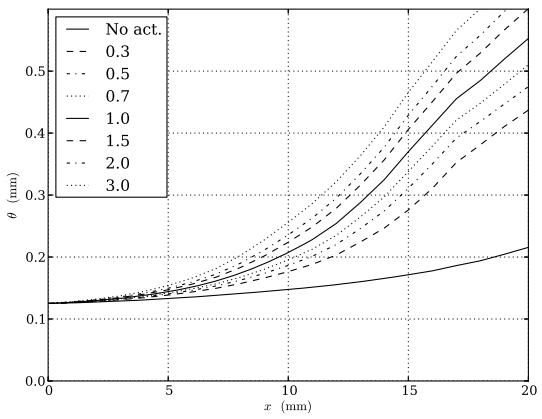

Fig. 20. Momentum thickness growth for cases without actuation and with actuation at fixed frequency with varying energy per pulse.

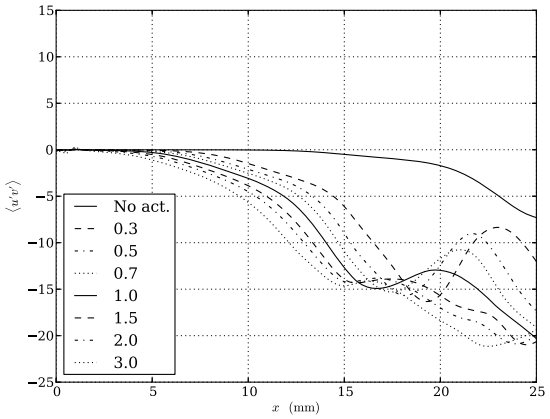

Fig. 21. Reynolds stress growth for cases without actuation and with actuation at fixed frequency with varying energy per pulse.

at which location) and should be determined in more detailed investigation for each specific case.

V. Conclusions

A numerical investigation of the excitation of a free shear layer with nanosecond plasma actuators has been carried out. The qualitative results are similar to those obtained in the experimental visualizations of [7]. Coherent vortex structures similar to those found in the experiments have been observed. Large increases in momentum thickness and Reynolds stress of the shear layer due to actuation have been observed, and the influence of actuation frequency and amplitude quantified. Furthermore, it was found that the computed growth rates only partially correspond to those from linear stability theory, indicating there are non-conventional mechanisms involved in the breakup of shear layers via nanosecond pulse actuation. The results should help to clarify the fundamental principles of nanosecond plasma control, and should be helpful for actuator design.

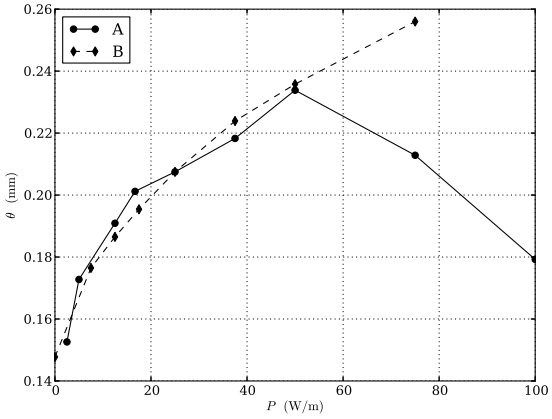

Fig. 22. Momentum thickness θ at station $x = 10\,\mathrm{mm}$ vs. discharge power P. A — at constant energy per pulse and varying frequency, B — at constant frequency 1000 Hz and varying energy per pulse.

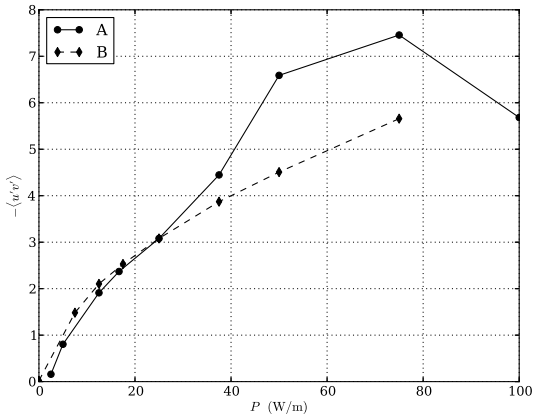

Fig. 23. Reynold stress $\langle u'v' \rangle$ at station $x = 10\,\mathrm{mm}$ vs. discharge power P. A — at constant energy per pulse and varying frequency, B — at constant frequency 1000 Hz and varying energy per pulse.

APPENDIX
CALCULATION OF THEORETICAL GROWTH RATES

This appendix describes numerical procedure used to obtain theoretical predictions of growth rates from linear stability theory. A well-developed method of such predictions is an Orr-Sommerfeld equation. Given mean velocity profile $U(y)$, the equation

$$\left(\frac{d^2}{dy^2} - \alpha^2\right)^2 \phi = iRe\left[(\alpha U - \omega)\left(\frac{d^2}{dy^2} - \alpha^2\right)\phi - \alpha U''\phi\right] \tag{8}$$

where ϕ is a stream function of a disturbance, allows to determine spatial complex wavenumber α as a function of angular frequency ω. In current work, equation has been discretised used finite differences in the following way:

$$\left(\alpha^4\mathbf{I} + \alpha^3\mathbf{C_3} + \alpha^2\mathbf{C_2} + \alpha\mathbf{C_1} + \mathbf{C_0}\right)\phi = 0 \tag{9}$$

$$\begin{aligned}
\mathbf{C_3} &= iReU\mathbf{I} \\
\mathbf{C_2} &= -(iRe\omega\mathbf{I} + 2\mathbf{L}) \\
\mathbf{C_1} &= iRe(\mathbf{L}U - U\mathbf{L}) \\
\mathbf{C_0} &= \mathbf{L}^2 + iRe\omega\mathbf{L}
\end{aligned} \tag{10}$$

where $\mathbf{L}$ is a matrix of finite differences second derivative operator $\frac{d^2}{dy^2}$.

This is an non-linear eigenvalues problem, which can be solved using companion matrix method as described in [9]. Following this method, the above eigenvalue problem can be rewritten in the form

$$\left[\begin{pmatrix} -\mathbf{C_3} & -\mathbf{C_2} & -\mathbf{C_1} & -\mathbf{C_0} \\ \mathbf{I} & \mathbf{0} & \mathbf{0} & \mathbf{0} \\ \mathbf{0} & \mathbf{I} & \mathbf{0} & \mathbf{0} \\ \mathbf{0} & \mathbf{0} & \mathbf{I} & \mathbf{0} \end{pmatrix} - \alpha\mathbf{I}\right]\begin{pmatrix} \alpha^3\phi \\ \alpha^2\phi \\ \alpha\phi \\ \phi \end{pmatrix} = 0 \tag{11}$$

In this formulation, we have linear eigenvalues problem of size $4n$ where n is the size of original non-linear problem, determined by the size of the mesh used for discretisation. This problem can be solved using conventional methods for eigenvalues problems. The last quarter of the eigenvector of companion matrix is an eigenvector of Orr-Sommerfeld problem. It should be noted, that non all the obtained eigenvalues have physical meaning, and there are branches of continuous spectrum, as described in [10]. After excluding unphysical eigenvalues, we select an eigenvalue α_1 having the lowest imaginary part. And finally, spatial growth rate

$$g = -\operatorname{Im}\alpha_1 \tag{12}$$

REFERENCES

[1] D. V. Roupassov, A. A. Nikipelov, M. M. Nudnova, and S. A. Yu., "Flow separation control by plasma actuator with nanosecond pulsed-periodic discharge," *AIAA Journal*, vol. 47, no. 1, 2009.

[2] I. V. Adamovich, I. Choi, N. Jiang, J.-H. Kim, S. Keshav, W. R. Lempert, E. Mintusov, M. Nishihara, M. Samimy, and M. Uddi, "Plasma assisted ignition and high-speed flow control: non-thermal and thermal effects," *Plasma Sources Sci. Technol.*, no. 18, 2009.

[3] M. M. Nudnova, S. V. Kindysheva, N. L. Aleksandrov, and A. Y. Starikovskiy, "Rate of plasma thermalization of pulsed nanosecond surface dielectric barrier discharge," in *48th AIAA aerospace Sciences Meeting including the New Horizons Forum and Aerospace Exposition*, no. 0465, 2010.

[4] J. Little, *High-Lift Airfoil Separation Control with Dielectric Barrier Discharge Plasma Actuators*. PhD thesis, The Ohio State University, 2010.

[5] T. Unfer and J. P. Boeuf, "Modelling of a nanosecond surface discharge actuator," *J. Phys. D: Appl. Phys.*, vol. 42, 2009.

[6] J. Little and M. Samimy, "High-lift airfoil separation with dielectric barrier discharge plasma actuation," *AIAA journal*, vol. 48, no. 12, 2010.

[7] G. Correale, I. Popov, A. Rakitin, A. Starikovskii, S. Hulshoff, and L. Veldhuis, "Flow separation control on airfoil with pulsed nanosecond discharge actuator," in *49th AIAA Aerospace Sciences Meeting including the New Horizons Forum and Aerospace Exposition, Orlando, Florida*, 2011.

[8] C.-M. Ho and P. Huerre, "Perturbed free shear layers," *Ann. Rev. Fluid Mech*, vol. 16, pp. 365–424, 1984.

[9] T. J. Bridges and P. J. Morris, "Defferential eigenvalue problems in which the parameter appears nonlinearly," *Journal of Computational Physics*, vol. 55, pp. 437–460, 1984.

[10] H. Salwen and C. E. Grosch, "The continuous spectrum of the Orr-Sommerfeld equation. Part 2: Eigenfunction expansions," *J. Fluid Mech.*, vol. 104, pp. 445–465, 1981.

[11] J. Little, K. Takashima, M. Nishihara, I. Adamovich, and M. Samimy, "High lift airfoil leading edge separation control with nanosecond pulse driven dbd plasma actuators," in *5th Flow Control Conference 28 June - 1 July 2010, Chicago, Illinois*, 2010-4256.

[12] D. V. Roupassov, A. A. Nikipelov, M. M. Nudnova, and A. Y. Starikovskii, "Flow separation control by plasma actuator with nanosecond pulse periodic discharge," in *46th AIAA Aerospace Sciences Meeting and Exhibit*, 2008-1367.
[13] J. Little, K. Takashima, M. Nishihara, I. Adamovich, and M. Samimy, "High lift airfoil leading edge separation control with nanosecond pulse driven dbd plasma actuators," in *5th Flow Control Conference*, 2010.
[14] A. Y. Starikovskii, A. A. Nikipelov, M. M. Nudnova, and D. V. Roupassov, "SDBD plasma actuator with nanosecond pulse-periodic discharge," *Plasma Sources Science and Technology*, vol. 18, no. 3, p. 034015, 2009.